Journal of Cleaner Production 265 (2020) 121823

Contents lists available at ScienceDirect

Journal of Cleaner Production

journal homepage: www.elsevier.com/locate/jclepro

# Assessment of design constraints for the Duplex Stirling Refrigerator with imperfect regeneration

Bahadır Doğan

*Department of Mechanical Engineering, School of Engineering and Architecture, Eskişehir Osmangazi University, 26480, Eskişehir, Turkey*

ARTICLE INFO

*Article history:*
Received 6 February 2020
Received in revised form
18 March 2020
Accepted 19 April 2020
Available online 25 April 2020

Handling Editor: Jin-Kuk Kim

*Keywords:*
Imperfect regeneration
Duplex Stirling
Coefficient of performance
Refrigeration

ABSTRACT

Duplex Stirling refrigerators are the alternative cycles to the conventional vapor refrigeration cycles with their high efficient, low noise, and low emission characteristics. It consists of a Stirling heat engine and a Stirling refrigerator in a mono-block construction that operates by a power piston. In this particular study, the effect of imperfect regeneration on the performance of the duplex Stirling refrigerator is determined analytically while helium is the working fluid. The polytropic heat transfer processes are chosen instead of isothermal processes to get a more realistic approach. Various temperature and compression ratios are taken into account for the refrigerator side of the duplex system and the required compression ratio of the heat engine is determined by using the work equality constraint. The combined effects of the regenerator effectiveness, temperature and compression ratios on the performance of the duplex system are assessed. The results of the parametric analysis are presented in terms of heat removal from the refrigerated space, coefficient of performance of the refrigerator side, work consumed by the system, heat addition to the engine side, thermal efficiency and overall system performance.

© 2020 Elsevier Ltd. All rights reserved.

## 1. Introduction

The Stirling engine designed by Robert Stirling in 1816 is one of the important models for energy resource utilization, power production, refrigeration, and space cooling applications. Stirling engines are capable of adapting to the existing systems with their high efficient, low noise, and low emission characteristics. Stirling engines and refrigerators are designed as an alternative clean cycle to the steam power and vapor compression refrigeration cycles. Today it still draws attention by different types such as Duplex Stirling Refrigerator (DSR) with its integration flexibility to varying sources and systems including environmental ones.

Fig. 1 shows the schematic of the DSR which was firstly introduced by Sunpower corporation (Penswick and Urieli (1984)) and was reported by several papers in the early 1990s (Berchowitz and Shonder (1991); Chen and Beale (1993)). As shown, a power piston takes place between the engine and the refrigerator side in a back-to-back configuration and it is associated with two free pistons called displacer. The heat engine side produces power by using fuel such as natural gas, helium, air, or carbon monoxide as the working fluid and drive the refrigerator side. Although there are not many studies related to the duplex Stirling cycles in the available literature until 2000, the interest on the duplex Stirling cycle has increased with a project proposed by NASA (Dyson (2012); Dyson and Bruder (2010)). The researchers studied the DSR to cool the electronic equipment used for the long-lived Venus lander.

Additionally, a linear model was proposed (Newman and Buckmaster (2011)) to predict the thermodynamic behavior of the DSR. Recent investigations have shown that innovative designs for the duplex Stirling cycles are being studied. A new configuration was proposed to keep the displacement of the power piston for the reliability of the duplex Stirling cycle (Hu et al. (2017)). Another new configuration was presented by considering a resonance tube to associate the Stirling heat engine and the Stirling cooler (Li et al. (2017)).

The ideal Stirling cycle includes isochoric compression and expansion, isothermal heat addition and rejection, and idealistic regeneration processes in theory. Researchers have attempted to obtain more realistic results by taking into account the friction losses, expansion and compression irreversibilities, and imperfect regeneration in this theoretical system. Blank et al. (1994) conducted a power analysis on the endoreversible Stirling cycle by taking into account the irreversible external heat transfer process. Chen et al. (1998) generated a linearized regenerative heat loss model for a solar-driven Stirling engine and determined the optimal operating temperature

*E-mail addresses:* bdogan@ogu.edu.tr, bahadirrdogan@gmail.com.

https://doi.org/10.1016/j.jclepro.2020.121823
0959-6526/© 2020 Elsevier Ltd. All rights reserved.

**Nomenclature**

| | |
|---|---|
| $C_p$ | specific heat at constant pressure, kJ/(kgK) |
| $C_v$ | specific heat at constant volume, kJ/(kgK) |
| *COP* | coefficient of performance |
| *DSR* | Duplex Stirling Refrigerator |
| $k$ | ratio of the specific heats |
| $m$ | mass, kg |
| $n$ | polytropic exponent |
| $Q^*$ | heat transfer, J |
| $Q$ | dimensionless heat transfer |
| $R$ | gas constant, kJ/(kgK) |
| $r$ | compression ratio, $V_{max}/V_{min}$ |
| $T$ | temperature, K |
| $W^*$ | work, J |
| $W$ | dimensionless work |
| $V$ | volume, $m^3$ |

*Greek letters*

| | |
|---|---|
| $\varepsilon$ | effectiveness of the regenerator |
| $\eta$ | thermal efficiency of the heat engine |
| $\tau$ | temperature ratio, $T_{min}/T_{max}$ |

*Subscripts*

| | |
|---|---|
| *C* | compression |
| *H* | heat engine side |
| *overall* | duplex unit |
| *p* | constant pressure |
| *R* | refrigerator side |
| *reg* | Regenerator |
| *rev* | Reversible |
| *th* | Thermal |
| *v* | constant volume |

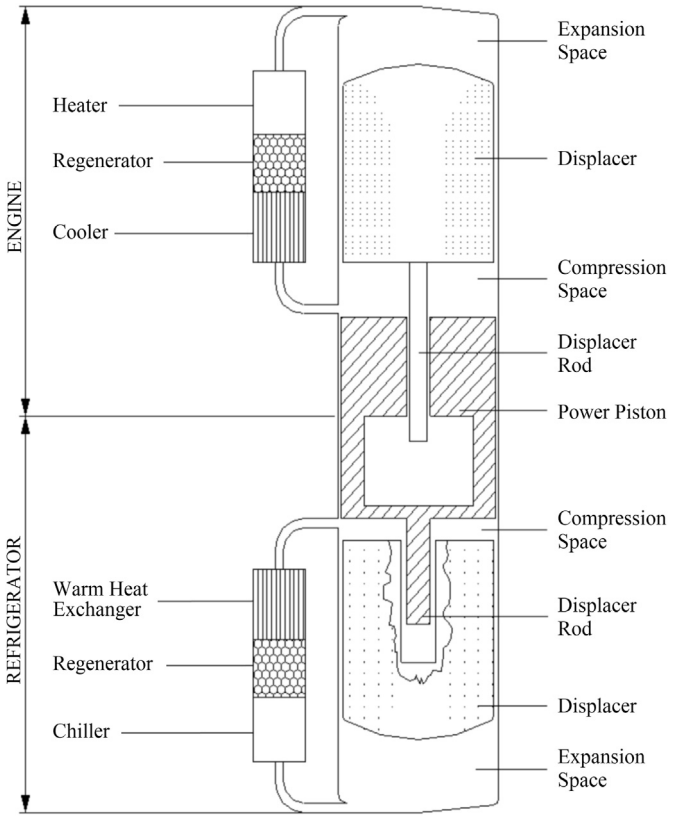



**Fig. 1.** Schematic of the Duplex Stirling Refrigerator (DSR).

and the maximum efficiency of the engine. Wu et al. (1998) examined the effects of irreversibilities during the regeneration process on the performance of the Stirling engine. De Waele and Liang (2008) presented an analytical study to determine the optimum performance of a split type Stirling refrigerator by considering the friction losses in the regenerator. Razani et al. (2010) proposed a thermodynamic model for a Stirling refrigerator considering the flow and heat transfer irreversibilities in the regenerator.

Kaushik and Kumar (2000) studied on the regenerative losses for an endoreversible Stirling engine In the next study, Kaushik and Kumar (2001) optimized the heat losses during the regeneration process of the Stirling and Ericsson heat engines. Kaushik et al. (2002) investigated the performance of Stirling and Ericsson heat pumps. It was noted that the effect of internal irreversibilities on the performance of the heat pumps is more dominant than the external irreversibilities. Kaushik et al. (2003) studied a Stirling heat engine by considering the effect of regenerative heat loss.

Kongtragool and Wongwises (2006) provided a model for heat losses during the regeneration process of a Stirling heat engine. It was noted that the thermal efficiency is effected by both dead volumes and the regenerator performance. Tlili et al. (2008) established a numerical model for a Stirling engine to determine the effects of regenerative irreversibility. Formosa and Despesse (2010) presented an analytical model that considers the heat losses and the irreversibilities of the engine to get a more realistic approximation. The optimal values of the regenerator length and regenerator effectiveness were determined.

Costa et al. (2014) designed a test unit and generated a numerical code to determine the heat transfer and pressure drop characteristics of a Stirling engine regenerator for different porosity and flow boundary conditions. Gheith et al. (2014) analyzed a gamma type Stirling engine and noted that the asymmetric design of the engine consumes a proportion of thermal energy in the regenerator. Ding et al. (2015) built a finite time thermodynamics analysis method to optimize a Stirling engine by illustrating the effects of heat leakage, and regenerative and mechanical losses. Li et al. (2015) studied a micro-channel type regenerator of a Stirling cycle to prevent high frictional losses. Liao and Lin (2015) analyzed the regenerative losses for a solar-driven Stirling engine. Ahmadi et al. (2016) used finite time thermodynamic analysis to determine the output power and the thermal efficiency of the Stirling heat engine by considering the regenerative heat losses. Arora et al. (2016) investigated the optimal value of the regenerator effectiveness for a solar-driven Stirling engine by using a genetic algorithm. Dai et al. (2018) reported the regeneration effectiveness and its limitations for a Stirling cycle by using finite-time thermodynamics.

A thermodynamic model was proposed to determine the performance bounds of the DSR in a wide range of temperature and compression ratios (Erbay et al. (2017)). At the second step, authors (Doğan et al. (2018)) generated the model for different couples of working fluid to determine the thermodynamic behavior of the DSR. Both of the studies considered the regeneration process as perfect. There is only one study that takes into account the

regenerative heat loss for a duplex Stirling cycle in the open literature. Dai et al. (2019) proposed a thermodynamic model for a DSR by considering the power and cycle time equalities.

Varying types of Stirling engines have been investigated from different aspects by the researchers in the last decades. Duplex Stirling is one of a kind application that allows benefiting from two of these engines, which are constructed in a back to back configuration. As it could be seen above, there has not been an article that addresses the combined effect of parameters including regenerator effectiveness, temperature, and compression ratios on the performance of the duplex Stirling system in the open literature. Therefore, the effects of operational and constructional parameters on the performance of the DSR are investigated by focusing on the regenerator effectiveness in this study. An analytical investigation is accomplished to reveal the effect of the regenerator effectiveness of both heat engine and refrigeration sides. The outcomes of the study will allow going one more step forward by providing necessary information about the combined effect of the parameters on the performance of the DSR by implementing the regenerator effectiveness inside.

## 2. Mathematical model of the thermodynamic analysis

Fig. 2 and Fig. 3 illustrate the *T-s* and the *P–V* diagrams for the refrigerator and the heat engine sides of the DSR. The cycle $1_R2_R3_R4_R1_R$ represents the refrigerator side of the duplex Stirling cycle with a perfect regeneration process which has the minimum temperature of $T_{2R}$, as shown in Fig. 2. $T'_{1R}$ and $T'_{3R}$ symbolize the temperatures at the end of the constant volume processes due to the imperfect regeneration.

In this study, polytropic processes are chosen instead of isothermal expansion and compression processes for a more realistic approach by taking into account the temperature difference in the regenerator. The exponent of the polytropic expansion process ($n_R$) is derived as a function of the exponent of polytropic compression process ($n_{CR} = 1.10$), compression ratio $r_R = (V_{3R}/V_{4R}) > 1$, temperature ratio $\tau_R = (T_{2R}/T_{4R}) < 1$, and the effectiveness of the regenerator $\varepsilon_{reg,R}$.

The cycle $1_H2_H3_H4_H1_H$ represents the heat engine cycle of the DSR with a perfect regeneration process which has the highest temperature of $T_{4H}$, as shown in Fig. 3. Similar to the refrigerator side $T'_{1H}$ and $T'_{3H}$ symbolize the temperatures at the end of the constant volume processes due to the imperfect regeneration, and $T_{1H}$ and $T_{3H}$ are the temperatures at the exit of the regenerator after a perfect regeneration process. The polytropic expansion and compression processes are selected instead of isothermal processes. $n_{CH}$ and $n_H$ symbolize the polytropic exponents for the compression and the expansion processes, respectively. $n_{CH}$ is

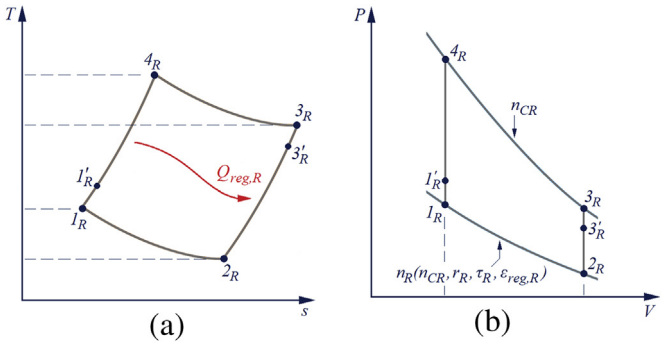



**Fig. 2.** (a) *T-s* and (b) *P–V* diagrams of the refrigerator side.

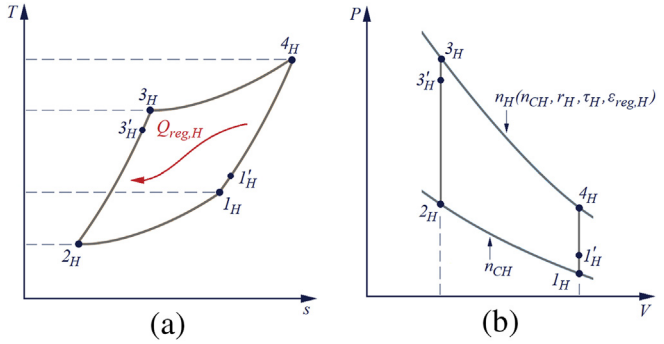



**Fig. 3.** (a) *T-s* and (b) *P–V* diagrams of the heat engine side.

constant as 0.85 and $n_H$ is derived as a function of the polytropic exponent for the compression process $n_{CH}$, compression ratio $r_H = (V_{1H}/V_{2H}) > 1$, temperature ratio $\tau_H = (T_{2H}/T_{4H}) < 1$, and the effectiveness of the regenerator, $\varepsilon_{reg,H}$.

The heat engine and the refrigeration cycle are connected in a back-to-back configuration with a power piston associated with two free pistons as shown in Fig. 1. It is assumed that the work output of the heat engine is used to drive the refrigerator side by considering work equality. In the following section, thermodynamic analysis of the DSR is performed under closed system approximation for the heat engine and the refrigerator sides. The irreversible heat transfer process and the flow friction losses in the regenerators are represented by regenerator effectiveness which is given in Eqs. (1) and (8) for the heat engine and refrigerator sides, respectively. The polytropic exponents of $n_H$ and $n_R$ are determined as the functions of regenerator effectiveness, temperature ratio, and compression ratio as seen in Eq. (2) and Eq. (9). Therefore, varying the regenerator effectiveness, temperature ratio, and compression ratio affect the properties of the whole cycle. According to the previous experience (Erbay et al. (2017); Doğan et al. (2018)), helium is selected as the working fluid of both cycles at equal quantity. The thermophysical properties of helium are considered as constant and are given in Table 1.

The effectiveness of the regenerator for the refrigerator side expressed in Eq. (1).

$$\varepsilon_{reg,R} = \frac{T'_{3R} - T_{2R}}{T_{4R} - T_{1R}} \tag{1}$$

The polytropic exponent of the expansion process ($n_R$) for the refrigerator side, which is derived by using Eq. (1), is given in Eq. (2).

$$n_R = 1 + \frac{ln\left\{\frac{1}{\tau_R}\left[1 - \frac{r_R^{(1-n_{CR})} - \tau_R}{\varepsilon_{reg,R}}\right]\right\}}{ln(r_R)} \tag{2}$$

The heat removal from the refrigerated space and its dimensionless form are expressed as in Eqs. (3) and (4), respectively.

**Table 1**
The properties of helium.

| $R$ [kJ/kgK] | $C_p$ [kJ/kgK] | $C_v$ [kJ/kgK] | $k$ |
|---|---|---|---|
| 2.08 | 5.19 | 3.11 | 1.67 |

$$Q_L^* = m_R C_v T_{4R} \frac{(k-n_R)}{(1-n_R)} \tau_R \left(1 - r_R^{n_R-1}\right) \tag{3}$$

$$Q_L = \frac{Q_L^*}{m_R C_v T_{4R}} \tag{4}$$

The work consumed by the refrigerator is given in Eq. (5) and it is expressed in a dimensionless form in Eq. (6).

$$W_{R,net}^* = m_R (k-1) C_v T_{4R} \left[ \frac{n_{CR}}{n_{CR}-1} \quad 1 - \frac{1}{r_R^{n_{CR}-1}} \right) - \frac{n_R}{1-n_R} \tau_R \left(1 - r_R^{n_R-1}\right) \Bigg] \tag{5}$$

$$W_R = \frac{W_{R,net}^*}{m_R C_v T_{4R}} \tag{6}$$

The coefficient of performance for the refrigerator cycle is given in Eq. (7).

$$COP_R = \frac{Q_L}{W_R} \tag{7}$$

The effectiveness of the regenerator for the heat engine side expressed in Eq. (8).

$$\varepsilon_{reg,H} = \frac{T_{3H}^{'} - T_{2H}}{T_{4H} - T_{1H}} \tag{8}$$

The polytropic exponent of the expansion process ($n_H$) for the heat engine side is derived by considering Eq. (8) and is given in Eq. (9).

$$n_H = 1 + \frac{ln\left[\tau_H + \varepsilon_{reg,H}\left(1 - \tau_H r_H^{(1-n_{CH})}\right)\right]}{ln(r_H)} \tag{9}$$

The heat addition to the heat engine side is given in Eq. (10) and it is expressed in a dimensionless form in Eq. (11).

$$Q_H^* = m_H C_v T_{4H} \frac{(k-n_H)}{(1-n_H)} \left(1 - r_H^{n_H-1}\right) \tag{10}$$

$$Q_H = \frac{Q_H^*}{m_H C_v T_{4H}} \tag{11}$$

The work output of the heat engine is given in Eq. (12) and it is expressed in a dimensionless form in Eq. (13).

$$W_{H,net}^* = m_H (k-1) C_v T_{4H} \left[ \frac{n_H \left(1 - r_H^{n_H-1}\right)}{(1-n_H)} - \tau_H n_{CH} \frac{\left(r_H^{1-n_{CH}} - 1\right)}{(1-n_{CH})} \right] \tag{12}$$

$$W_H = \frac{W_{H,net}^*}{m_H C_v T_{4H}} \tag{13}$$

The thermal efficiency of the heat engine is given in Eq. (14).

$$\eta_{th} = \frac{W_H}{Q_H} \tag{14}$$

The overall performance coefficient of the duplex system is determined in Eq. (15) by considering the performances of both heat and refrigerator sides.

$$COP_{overall} = \eta_{th} COP_R \tag{15}$$

Finally, the performances of the refrigerator and heat engine side are limited separately in the second law of thermodynamics point of view by Eqs. (16) and (17).

$$COP_{R,rev} = \left(\tau_R^{-1} - 1\right)^{-1} \tag{16}$$

$$\eta_{th,rev} = 1 - \tau_H \tag{17}$$

The comprehensive parametric investigation of the DSR has carried out with regard to calculation procedure given in Fig. 4. As it is presented, there is a sequence that has to be followed during the calculations of the parameters and the unknowns either for the refrigeration side or the correspondent of them for the heat engine side of the duplex unit. The initial step of the entire parametric analysis is the determination of the polytropic exponent $n_R$ within the limits of the parameters ($\varepsilon_R$, $\tau_R$, $r_R$, $n_{CR}$) that is bounded to. After the determination of the $n_R$, the cooling load ($Q_L$) and required work ($W_R$) are calculated, which are the functions of polytropic exponents, temperature ratio, compression ratio, and regenerator's efficiency. After finding the $Q_L$ and $W_R$, the following step is the calculation of the refrigeration side's performance $COP_R$ as their function. The final stage of the calculations for the refrigeration side is the decision of $COP_R$ 's consistency with the second law of thermodynamics, if it is beyond the limits of the reversible cycle than that the particular set of parameters is eliminated and not included to the presented data in the following calculations, if not they are plotted on the given figures.

The calculations for the adjunct side of this duplex system begins with the determination of the heat engine side' compression ratio $r_H$ is derived from the produced work that has to be exactly the same amount consumed by the refrigeration side. In the following, polytropic exponent ($n_H$) is found within the limits of the parameters ($\varepsilon_H$, $\tau_H$, $r_H$, $n_{CH}$). As a further step the heat addition is determined and the thermal efficiency of the heat engine is calculated. Similar second law consistency is examined as conducted in the refrigeration side, and the calculated amount is compared with the reversible efficiency which is a constraint for the applicable designs. After the comparison, if the calculated value is above the reversible limits than that value is discarded and not presented in the figures as a possible design condition.

After the determination of possible working conditions and efficiencies for both sides, the overall performance of the integrated system is calculated to find out the performance of the entire system.

## 3. Results and discussion

Parametric performance assessment for a DSR with imperfect regeneration is presented in a wide range in this section. In the analysis, either the sole or combined effect of the regenerator effectiveness ($0.80 \leq \varepsilon \leq 1.00$), temperature ratios ($0.35 \leq \tau_R \leq 0.60$)

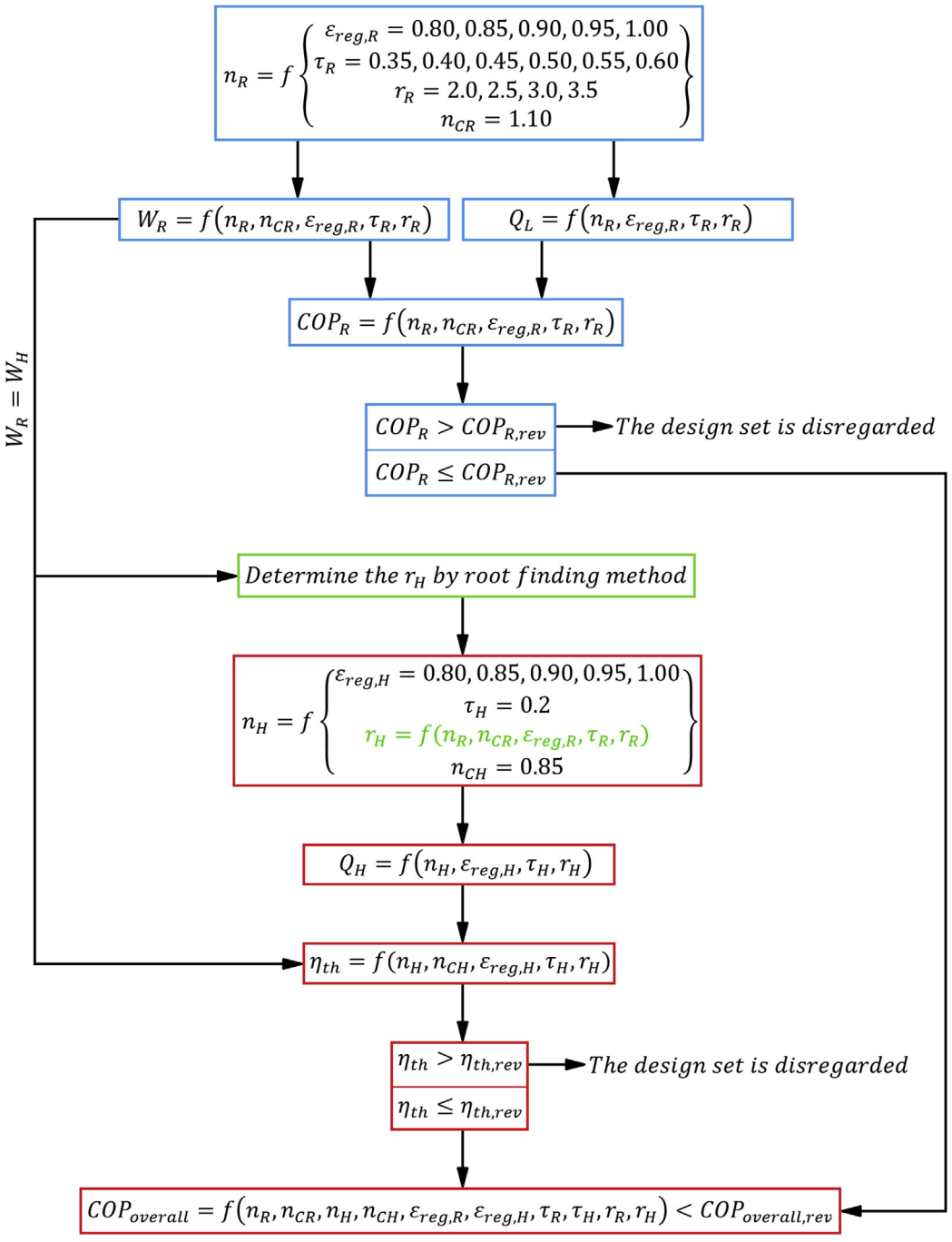



**Fig. 4.** The calculation procedure for the overall performance of the DSR.

and compression ratios ($2.0 \leq r_R \leq 3.5$) of the system are studied in detail.

The initial step for determination of the performance of the duplex system is being observed by the performance coefficient of refrigerator side, $COP_R$. The assessment of the $COP_R$ is examined according to the change of three basic parameters as $\varepsilon_R$, $\tau_R$ and $r_R$, and the results are summarized in Fig. 5. Each figure refers to different compression ratios of the refrigeration which changes from $r_R = 2.0$ to 3.5 while the regenerator effectiveness and temperature ratio varies in these figures in the range of $0.80 \leq \varepsilon_R \leq 1.00$ and $0.35 \leq \tau_R \leq 0.60$, respectively. As regards to the parametric plots, when $\tau_R$ increases, cooling load ascends too and as a consequence, performance gets better in all presented figures or compression ratio conditions.

It would be very useful to highlight the direction of the $\varepsilon_R$ change to prevent any misunderstanding, the lowest effectiveness value is on the right (solid line with circles) and the highest one is on the left (solid line with square), so the increment is from right to left. When a single compression ratio case is taken into account for a particular cooling load value, it could be observed that, when the regenerator effectiveness has higher values, the performance becomes better. The major reason for this is the reduction of the required work for that particular load which is compensated by the accession of effectiveness.

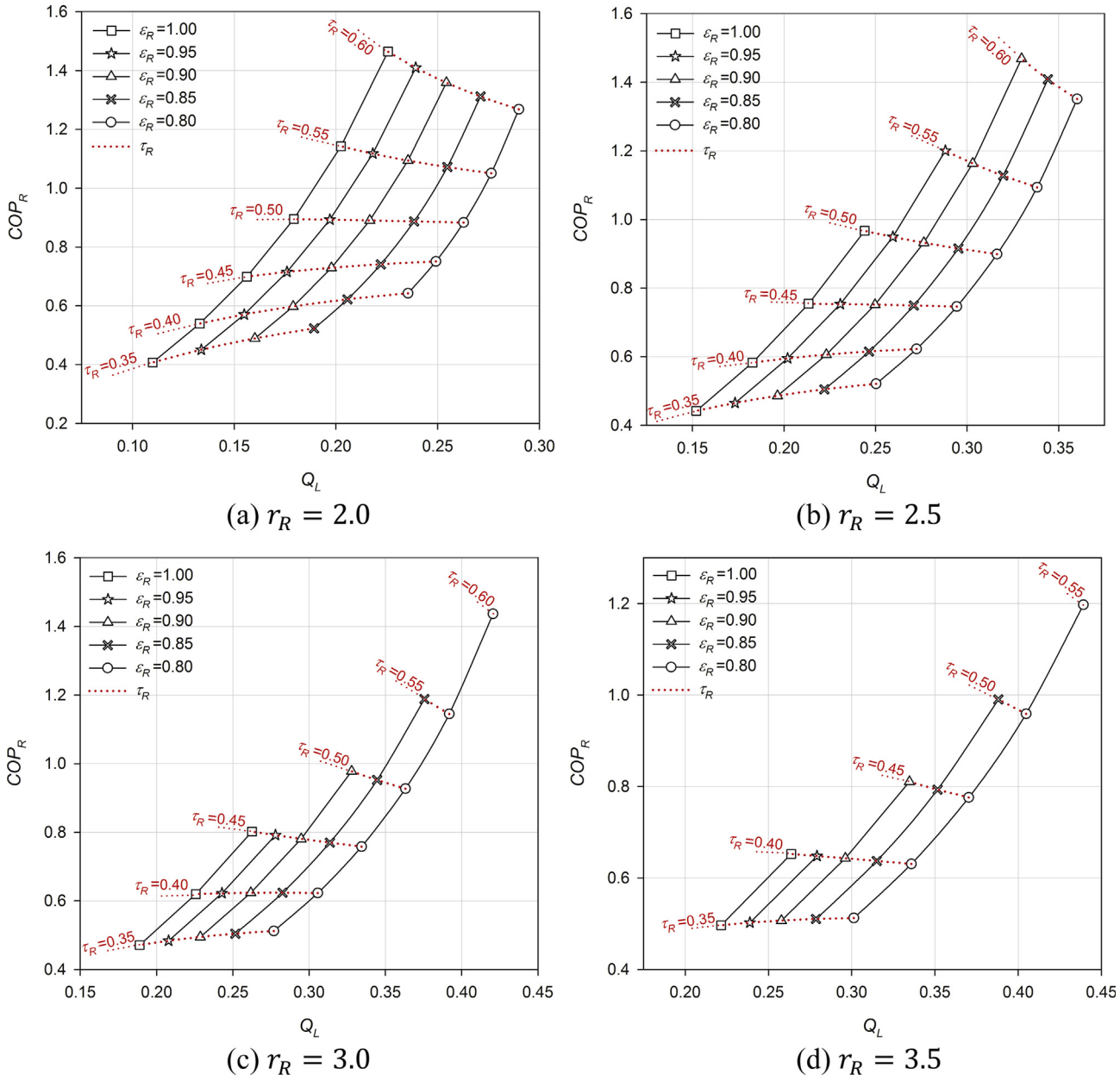



**Fig. 5.** The performance coefficient of the refrigerator side ($COP_R$) with respect to cooling load ($Q_L$) and the regenerator effectiveness ($\varepsilon_R$).

By considering the integrity of all figures (Fig. 5a–d), the impact of the compression ratio's increment on the performance coefficient is tentative. One important outcome as regard to this parametric investigation is the data which obeys to the second law of thermodynamics becomes lesser as the compression ratio increases. As the compression ratio ascends gradually, the data obtained within the limits of Carnot efficiency reduces gradually as a consequence of the combined effect of studied parameters. In particular, the DSR system with high regenerator efficiency ($\varepsilon_R$) and temperature ratio ($\tau_R$) begins to fail as the compression ratio increases. As regards to this combined effect of the crucial parameters, the data which is divergent with the second law become more when all three reaches to their highest values among the analyzed conditions (Fig. 5d).

When a particular performance coefficient is taken into account for a better comparison in Fig. 5a, it is seen that a couple of alternates emerge to attain the same performance. In the case of $COP_R = 1.0$, one of them is $\tau_R = 0.53$, and $Q_L = 0.19$ when the effectiveness of the regenerator on the refrigerator side, $\varepsilon_R = 1.00$; the second alternate to provide the same performance is obtained when $\tau_R = 0.55$, and $Q_L = 0.25$ where $\varepsilon_R = 0.85$. As seen the cooling load and the temperature ratio should be increased for the same $COP_R$, when the effectiveness of the regenerator is low. Similar cases could be seen in the rest of the figures (Fig. 5b–d) which have similar trends. It is understood that the systems with low regenerator effectiveness can only be applicable in case of higher temperature ratio and cooling load.

The importance of the target cooling load is underlined by the given diagram since the ranges of the $Q_L$ evolves from 0.11 to 0.28 (Fig. 5a) to 0.22–0.43 (Fig. 5b) which also relies on the combined effect of the parameters. If a closer look is taken to a particular cooling load value among these figures, such as $Q_L = 0.2$ the

performance values ($COP_R$) could be read approximately as; 1.14 at $r_R = 2.0$, 0.69 at $r_R = 2.5$ and 0.52 at $r_R = 3.0$ for the highest regeneration effectiveness ($\varepsilon_R = 1.00$). As it is noticed, if the system has lower cooling loads, then lower compression ratios would meet the requirement but as the cooling load target grows, lower $r_R$ values will be insufficient. In the same particular case, the importance of the regeneration effectiveness steps forward either, as the $\varepsilon_R$ drops down, it leads to a serious fall in the performance of the system. The $COP_R$ of the corresponding cooling load of $Q_L = 0.2$ at $r_R = 2.5$ (Fig. 5b), reduces from 0.69 to 0.59 range as $\varepsilon_R$ falls from 1.00 to 0.95.

The next step is the parametric observation of heat engine's performance ($\eta_{th}$) which is conducted by considering the effectiveness of regenerator ($\varepsilon_R = \varepsilon_H$), temperature ratio ($\tau_R$) and compression ratio ($r_R$) of the refrigeration side, as shown in Fig. 6.

The parameters that pertain to the refrigeration side are dominating the analysis for the heat engine side since the investigation is conducted for the determination of corresponding heat engine parameters which could meet the requirement of the refrigeration side. The necessary data used in the study is gathered by the following calculation sequence.

First, the cooling load is calculated, then the required work for this particular load individually is found without knowing the compression ratio of the heat engine side ($r_H$) as given in Fig. 4. Since the work consumed by the refrigeration is equal to the work output of the heat engine, the compression ratio ($r_H$) of heat engine which could maintain this equality is calculated by the root finding method. Finally, the heat input and thermal efficiency of the heat engine side ($\eta_{th}$) is calculated with $r_H$ found previously and $\tau_H = 0.2$.

The change in $r_H$ could be tracked on the figure by the green line. The thermal efficiency of the heat engine side ($\eta_{th}$) is plotted with

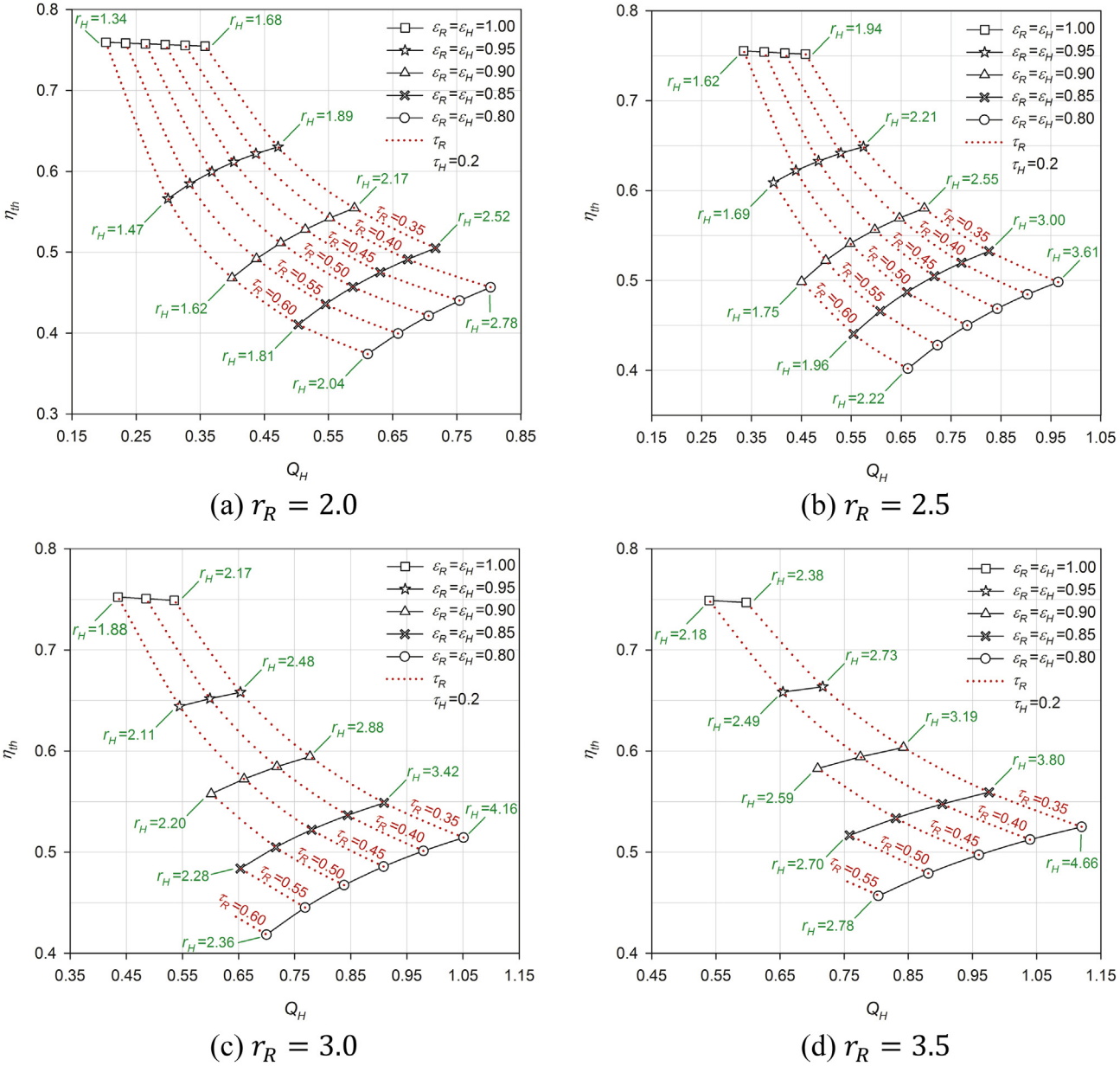



**Fig. 6.** The thermal efficiency of the heat engine side ($\eta_{th}$) meeting the requirement of the refrigerator side with respect to the heat input ($Q_H$) and the regenerator effectiveness ($\varepsilon_R = \varepsilon_H$).

respect to heat input for varying values of $\varepsilon_R = \varepsilon_H$ (0.80–1.00), $\tau_R$ (0.35–0.60) and $r_R$ (2.0–3.5). As it is obvious from Fig. 6 that the thermal efficiency of the heat engine becomes better in all compression ratios when the regenerator effectiveness ascends. The curve on the right which is drawn by a solid line with a circle is the lowest regenerator effectiveness ($\varepsilon_R = \varepsilon_H = 0.80$) and it grows from right to left where it ends up with a solid line with diamond ($\varepsilon_R = \varepsilon_H = 1.00$). As for the temperature ratio effect, the thermal efficiency increases as the temperature difference between the sources ascends. The mentioned trend could be observed in each figure of compression ratios ($r_R$=2.0–3.5) within almost the same range of limit values. Even though heat input and thermal efficiency evolve in similar ranges, it is very important to keep in mind that these are the correspondent data of the target cooling loads calculated previously. So while interpreting the figures, the reader should avoid considering the figures as alternate to each other.

Among all investigated cases given in Fig. 6a–d, the performance does not rely on a parameter solely, the combined effect of them instead. When the evolution of the plots observed, and focus on a particular temperature ratio such as $\tau_R = 0.35$, it is seen that the lower values of regenerators' effectiveness ($\varepsilon_R = \varepsilon_H$), needs higher compression ratios ($r_H$) on the heat engine side to achieve the targeted work equality. But it should be noted that the rise of the compression ratio leads to a fall on the thermal efficiency of the heat engine side ($\eta_{th}$), as a result of the decrement of the regenerator's contribution to the heat requirement for the production of the work on the heat engine side. Since this deficit can be compensated by the addition of more heat for the particular works, the thermal efficiency falls as a consequence of this natural process. As the compression ratio $r_R$ ascends gradually, the number of investigated conditions of the DSR that obeys the second law descends gradually too. The number of conditions which are against the second law grows as the compression ratio rises, in particular at the higher temperature ratios ($\tau_R$). It can be stated that the DSR operations start to fail once $\tau_R >$ 0.50 when compression ratio $r_R$ is 2.5, $\tau_R > 0.45$ when compression ratio $r_R$ is 3.0 and $\tau_R > 0.40$ when $r_R$ is 3.5. From the Carnot efficiency aspect, these ranges can be considered as the applicable thresholds of the DSR operations. The designs beyond these ranges are not applicable with regard to identified constraints.

The relation between $COP_R$ and $W_R$ is presented in Fig. 7 to show the impact of the work on the performance. The evolution of $COP_R$ versus $W_R$ is investigated with regard to $\varepsilon$ (0.80–1.00), $\tau_R$ (0.35–0.60) and $r_R$ (2.0–3.5) in the given ranges. To provide a better look at the big picture, all four sets are given in the same figure at once. Each set of data which belongs to an individual compression ratio ($r_R$) are colored independently from previous sets. The major relation which can be noted at first glance is the inverse proportion with the work and performance, as the work increases the performance reduces. So basically the conditions which make the work requirement higher, lead to a reduction in the performance of the refrigeration. As expected the regenerator effectiveness has a very important role in the performance, as the $\varepsilon_R$ increases, the performance becomes better. The highest value in each data set belongs to the highest effectiveness value. But unfortunately, it is not the only condition that would maintain higher performance. The performance is depended on to the combined effect of the given parameters ($\varepsilon_R$, $\tau_R$ and $r_R$). As the temperature difference increases between the sources ($\tau_R$ reduces), the $W_R$ascends which reduces the performance ($COP_R$) of the refrigerator.

The operational constraints due to the second law or Carnot efficiency emerges at this diagram once again. Even though a gradual increment can be expected when the first set of data which pertain to $r_R = 2.0$ is taken into account, the plotted data gradually reduces due to the inconsistency of them with the second law. If a closer look is taken to a particular value, the evolution and the combined effect of the parameters could be seen better. For instance, in Fig. 6a, for $W_R = 0.25$ in the compression ratio cluster for the $r_R = 2.0$. The performance value ($COP_R$) that correspond to this work value ($W_R = 0.25$) is 0.54 when $\varepsilon = 1.00$ and $\tau_R = 0.35$, while $COP_R$ is 1.06 when $\varepsilon = 0.85$ and $\tau_R = 0.55$. As it could be seen none of the parameters is sufficient to improve the performance solely, it can be low even the $\varepsilon_R$ has the highest and it can be high even if $\varepsilon_R$ is the lowest.

In Fig. 8, a similar examination is conducted to see the impact of the parameters ($\varepsilon_R$ , $\tau_R$ and $r_R$) via $W_R$ on to the overall system's performance $COP_{overall}$. Similar evolution trends are observed by some exceptions. By the increment of the $r_R$, as the regenerator

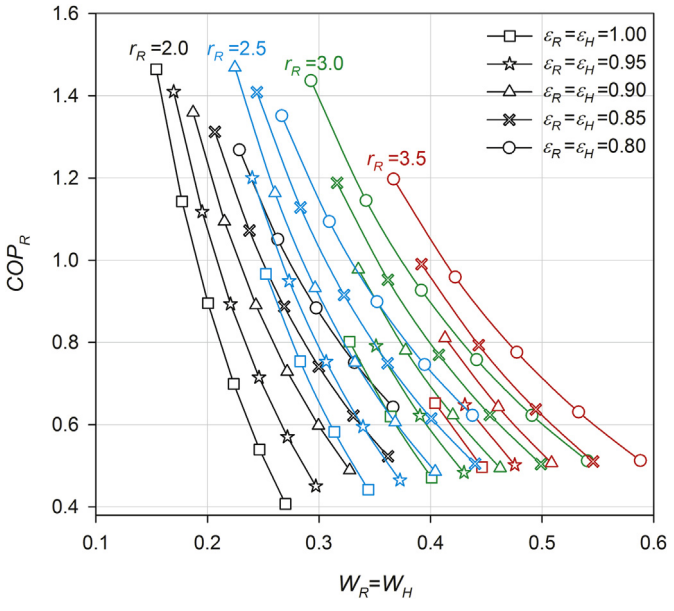



**Fig. 7.** The performance coefficient of the refrigerator side ($COP_R$) with respect to work consumed by the refrigerator side ($W_R$) under the work equality constraint.

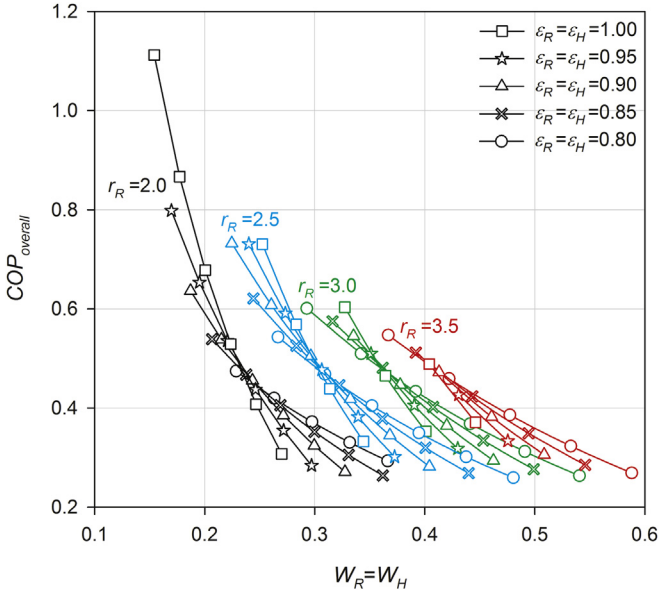



**Fig. 8.** The overall performance coefficient of the refrigerator side ($COP_{overall}$) with respect to work consumed by the refrigerator side ($W_R$) under the work equality constraint.

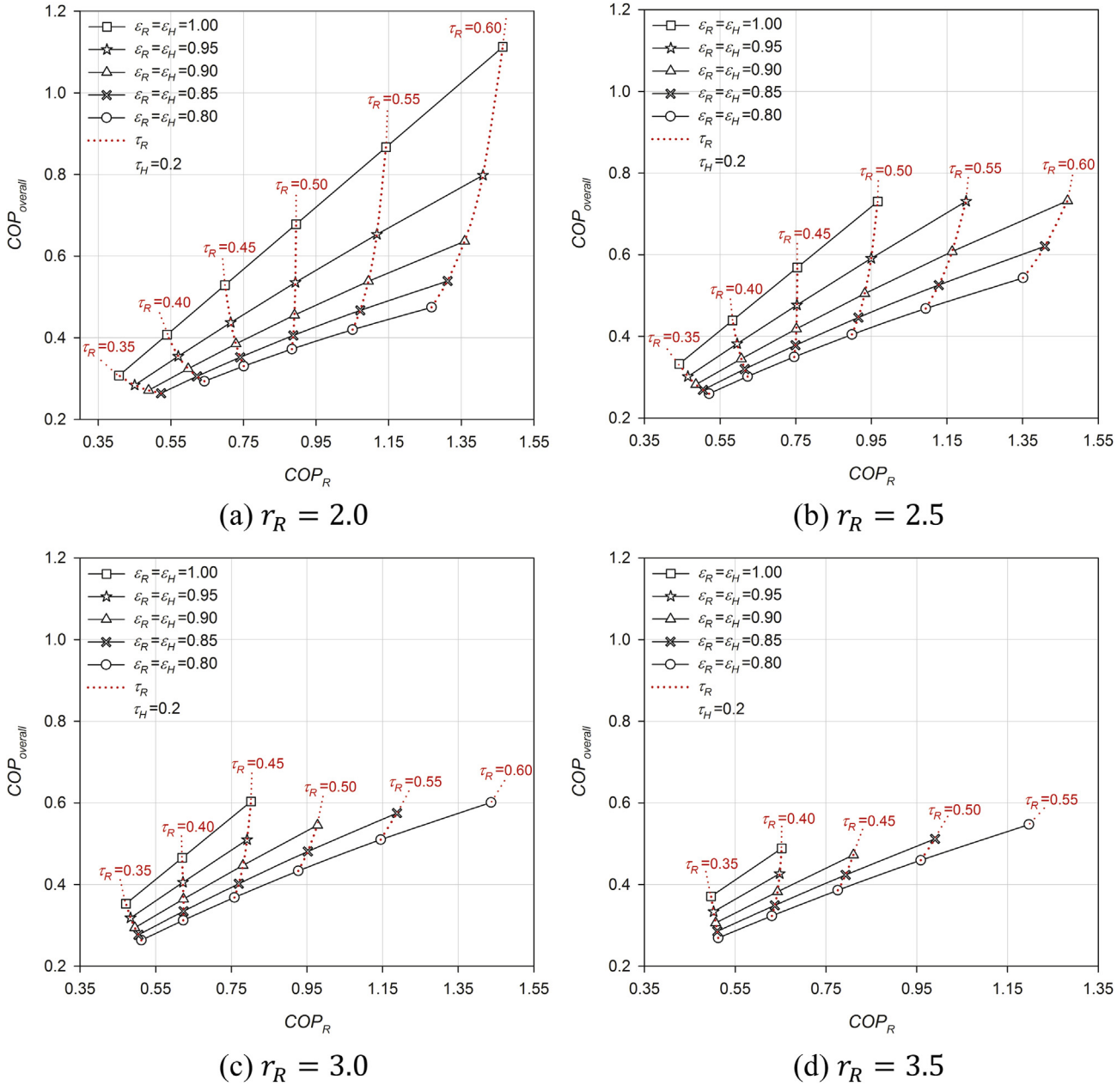



**Fig. 9.** The overall performance coefficient of the refrigerator side ($COP_{overall}$) with respect to overall performance coefficient of the refrigerator side ($COP_R$) and the regenerator effectiveness ($\varepsilon_R = \varepsilon_H$).

effectiveness approaches to 1.00, the system requires lesser work and performance improves. Besides, as the temperature difference increases the performance falls due to the increment of the work requirement.

Similar limitations as a consequence of the second law arose at this diagram too as per the earlier figures. Although all the investigated conditions obey the second law when $r_R$ is 2.0, the number of data which become against the Carnot efficiency ascends as the $r_R$ increases. Even though the overall trend of the evolution is in increment with regard to the rise of the compression ratio, this trend is not very noticeable since the data plotted in these clusters are getting less in each step gradually. For instance, when $r_R$ is 2.0, all six $\tau_R$ data can be displayed at $\varepsilon = 1.00$ since they don't disagree with the second law but as the $r_R$ increases from 2.5 to 3.5 the number of data that can be plotted by considering the law, reduces to 4, 3 and 2 respectively which makes it difficult to display the real impact of the compression ratio's increment on the overall performance. When the attention is paid on the clusters instead, the importance of the combined effect could be seen better since plots over crosses at a particular condition in every one of them. For instance, in the cluster of $r_R = 2.0$, when a closer look is taken to $W_R = 0.17$ it is seen that the correspondent overall performance of the DSR is $COP_{overall} = 0.86$ when $\varepsilon = 1.00$ and $\tau_R = 0.55$, the same $W_R = 0.17$ could be consumed (produced) by DSR when the performance $COP_{overall} = 0.76$ for $\varepsilon = 0.95$ and $\tau_R = 0.6$ either. The superiority of plot that pertains to $\varepsilon = 1.00$ changes to the one that belongs to $\varepsilon = 0.80$ in the rest of the investigated conditions. Once again it could be observed better on a particular case, for instance, when $W_R = 0.26$, the overall performance of DSR is 0.42 when $\varepsilon = 0.80$ and $\tau_R = 0.50$; while the overall performance of the system

becomes 0.29 when the $\varepsilon = 1.00$ and $\tau_R = 0.35$. This also underlines the importance of the coupling effect of the parameters for both sides instead of taking into account them separately as indicated in Fig. 7 and shows that different designs may be suitable for a certain overall performance coefficient. Thus, it is understood that the operating conditions are determining the dimensions of the DSR.

Finally, the overall performance of the system ($COP_{overall}$) is examined by considering the performance of the refrigerator side ($COP_R$). The change is observed by using the same parameters in the same ranges, $0.80 \leq \varepsilon \leq 1.00$, $0.35 \leq \tau_R \leq 0.60$, and $2.0 \leq r_R \leq 3.5$ as shown in Fig. 9. The overall trend about the impact of the parameters on the performance is seen in the figures. The conditions which improve the performance of the refrigerator side improves the performance of the overall system either. As the $\varepsilon$ grows from 0.80 to 1.00, the performance on both sides improves. The other leading factor, $\tau_R$ increment also positively affect the performance, as the temperature difference between the sources reduces, the performance improves either. The increase of the other parameter, $r_R$, which is shown individually this time, also makes the performance better as the compression ratio gradually increases. For instance, the $COP_R$ and $COP_{overall}$ values when $\varepsilon = 1.00$ and $\tau_R = 0.40$ are 0.40 and 0.54 at $r_R = 2.0$, 0.43 and 0.58 at $r_R = 2.5$, 0.46 and 0.61 at $r_R = 3.0$ and finally at $r_R = 3.5$, 0.48 and 0.65. This basic example also clearly shows the combined effect of the parameters on the performance of the sole system and duplex one. One other major impact of the imperfect regeneration arose when the temperature ratio between the sources of the refrigerator side ($\tau_R$) changes. For instance, in Fig. 9a, as the effectiveness values ($\varepsilon_R = \varepsilon_H$) varies in the range of 0.80–1.00, the impact of $\tau_R$ on the overall performance changes in different ranges.

For instance, when $\varepsilon_R$ and $\varepsilon_H$ falls from 1.00 to 0.80 for $\tau_R = 0.4$ value, the overall performance drops by half at this particular temperature ratio, while the change of $COP_{overall}$ occurs around one third at $\tau_R = 0.60$. This phenomenon is similar in other compression ratios for the refrigerator side (Fig. 9b–d). The inconsistency of the obtained data with the second law of thermodynamics appears in these figures set too. Like in the earlier figures the number of data that obeys to the second law reduces gradually as the compression ratio gradually increases. All the investigated temperature ratios are applicable only if the compression ratio ($r_R$) is 2.0, while the conditions with higher temperature ratios become less pertinent at the higher compression ratios. It can be reported that DSR operations start to fail once $\tau_R > 0.50$ when compression ratio $r_R$ is 2.5, $\tau_R > 0.45$ when compression ratio $r_R$ is 3.0 and $\tau_R > 0.40$ when $r_R$ is 3.5. In the range of the given constraints, the first inconsistencies emerge for $\varepsilon = 1.00$ which is followed by 0.95 in Fig. 9b, 0.90 and 0.85 in Fig. 9c and 0.8 in Fig. 9d. As it could be seen that, when the compression ratio reaches to 3.5, the possible design conditions becomes limited as compared to the lower $r_R$ values.

## 4. Conclusion

In this study, the assessment of the imperfect regeneration process for a DSR is presented in the thermodynamic point of view. The ultimate purpose of the study is to determine the effect of the imperfect regeneration process by taking into account the constructional and operational parameters for both refrigeration and heat engine sides. In the meantime, the heat engine side performance in terms of thermal efficiency and overall performance coefficient of the DSR is assessed by considering the same regenerator effectiveness for both sides. Even though the individual effect of the parameters on the duplex Stirling could be observed during the analytical study, more importantly, the overall performance of the duplex system relies on the combined effect of the parameters instead of their sole effect. By considering the combined effects of the regenerator effectiveness, temperature and compression ratios, it can be seen that the possible design sets are decreasing among the investigated cases in the second law of thermodynamics point of view when these parameters get higher values. In particular, even if the other parameters remain constant, only the increase in the compression ratio of the refrigerator side reveals the impossible design sets. It is found that the number of possible design sets is reduced by half within the investigated cases when the compression ratio of the refrigerator side increases from $r_R = 2.0$ to 3.5. The sole effect of the low regenerator effectiveness revealed that the higher temperature ratios were needed for the same performance coefficient. If the combined effect of the regenerator effectiveness, temperature and compression ratios are considered, some threshold ranges emerge for the applicability of DSR. The DSR operations start to fail when $r_R = 2.5$ and $\tau_R > 0.50$, $r_R = 3.0$ and $\tau_R > 0.45$, and $r_R = 3.5$ and $\tau_R > 0.40$. Therefore, the combined parametric effect considered in the present study has been the hearth of the duplex Stirling arrangement to be developed and extensively used in practice.

## Declaration of competing interest

The author of the manuscript entitled with "**Assessment of Imperfect Regeneration for the Performance of Duplex Stirling Refrigerator**" certify that they have NO affiliations with or involvement in any organization or entity with any financial interest (such as honoraria; educational grants; participation in speakers' bureaus; membership, employment, consultancies, stock ownership, or other equity interest; and expert testimony or patent-licensing arrangements), or non-financial interest (such as personal or professional relationships, affiliations, knowledge or beliefs) in the subject matter or materials discussed in this manuscript.

## CRediT authorship contribution statement

**Bahadır Doğan:** Visualization, Writing - original draft, Writing - review & editing.

## References


Ahmadi, M.H., Ahmadi, M.A., Mehrpooya, M., 2016. Investigation of the effect of design parameters on power output and thermal efficiency of a Stirling engine by thermodynamic analysis. Int. J. Low Carbon Technol. 11 (2), 141–156. https://doi.org/10.1093/ijlct/ctu030.

Arora, R., Kaushik, S.C., Kumar, R., Arora, R., 2016. Multi-objective thermo-economic optimization of solar parabolic dish Stirling heat engine with regenerative losses using NSGA-II and decision making. Int. J. Electr. Power Energy Syst. 74, 25–35. https://doi.org/10.1016/j.ijepes.2015.07.010.

Berchowitz, D.M., Shonder, J., 1991. Estimated Size and Performance of a Natural Gas Fired Duplex Stirling for Domestic Refrigeration Applications, 18th International Congress of Refrigeration, pp. 1350–1354. Montreal, Canada.

Blank, D.A., Davis, G.W., Wu, C., 1994. Power optimization of an endoreversible stirling cycle with regeneration. Energy 19 (1), 125–133. https://doi.org/10.1016/0360-5442(94)90111-2.

Chen, G., Beale, W.T., 1993. In: Thermally Actuated Duplex Free-Piston Stirling System for Domestic Cooling and Heating Applications, International Conference on CFCs and Halon Alternatives (Beijing, China).

Chen, J.C., Yan, Z.J., Chen, L.X., Andresen, B., 1998. Efficiency bound of a solar-driven Stirling heat engine system. Int. J. Energy Res. 22 (9), 805–812. https://doi.org/10.1002/(SICI)1099-114X(199807)22:9%3C805::AID-ER404%3E3.0.CO;2- (K ).

Costa, S.-C., Tutar, M., Barreno, I., Esnaola, J.-A., Barrutia, H., García, D., González, M.-A., Prieto, J.-I., 2014. Experimental and numerical flow investigation of Stirling engine regenerator. Energy 72, 800–812. https://doi.org/10.1016/j.energy.2014.06.002.

Dai, D., Liu, Z., Yuan, F., Long, R., Liu, W., 2019. Finite time thermodynamic analysis of a solar duplex Stirling refrigerator. Appl. Therm. Eng. 156, 597–605. https://doi.org/10.1016/j.applthermaleng.2019.04.098.

Dai, D.D., Yuan, F., Long, R., Liu, Z.C., Liu, W., 2018. Imperfect regeneration analysis of Stirling engine caused by temperature differences in regenerator. Energy Convers. Manag. 158, 60–69. https://doi.org/10.1016/j.enconman.2017.12.032.

De Waele, A.T.A.M., Liang, W., 2008. Basic dynamics of split Stirling refrigerators.

Cryogenics 48 (9–10), 417–425. https://doi.org/10.1016/j.cryogenics.2008.04.004.
Ding, Z.M., Chen, L.G., Sun, F.R., 2015. Performance optimization of a linear phenomenological law system Stirling engine. J. Energy Inst. 88 (1), 36–42. https://doi.org/10.1016/j.joei.2014.04.008.
Doğan, B., Ozturk, M.M., Erbay, L.B., 2018. Effect of working fluid on the performance of the duplex Stirling refrigerator. J. Clean. Prod. 189, 98–107. https://doi.org/10.1016/j.jclepro.2018.04.076.
Dyson, R., Bruder, G., 2010. Progress towards the development of a long-lived Venus lander duplex system. In: 8th Annual International Energy Conversion Engineering Conference. Nashville, United States. Paper ID: 20110012039.
Dyson, R.W., 2012. Terrestrial Applications of Extreme Environment Stirling Space Power Systems. Energytech, 2012 IEEE, Cleveland, OH, pp. 1–5.
Erbay, L.B., Ozturk, M.M., Doğan, B., 2017. Overall performance of the duplex Stirling refrigerator. Energy Convers. Manag. 133, 196–203. https://doi.org/10.1016/j.enconman.2016.12.003.
Formosa, F., Despesse, G., 2010. Analytical model for Stirling cycle machine design. Energy Convers. Manag. 51 (10), 1855–1863. https://doi.org/10.1016/j.enconman.2010.02.010.
Gheith, R., Aloui, F., Ben Nasrallah, S., 2014. Study of temperature distribution in a Stirling engine regenerator. Energy Convers. Manag. 88, 962–972. https://doi.org/10.1016/j.enconman.2014.09.043.
Hu, J.Y., Luo, E.C., Dai, W., Zhang, L.M., 2017. Parameter sensitivity analysis of duplex Stirling coolers. Appl. Energy 190, 1039–1046. https://doi.org/10.1016/j.apenergy.2017.01.022.
Kaushik, S.C., Kumar, S., 2000. Finite time thermodynamic analysis of endoreversible Stirling heat engine with regenerative losses. Energy 25 (10), 989–1003. https://doi.org/10.1016/s0360-5442(00)00023-2.
Kaushik, S.C., Kumar, S., 2001. Finite time thermodynamic evaluation of irreversible Ericsson and Stirling heat engines. Energy Convers. Manag. 42 (3), 295–312. https://doi.org/10.1016/s0196-8904(00)00063-7.
Kaushik, S.C., Tyagi, S.K., Bose, S.K., Singhal, M.K., 2002. Performance evaluation of irreversible Stirling and Ericsson heat pump cycles. Int. J. Therm. Sci. 41 (2), 193–200. https://doi.org/10.1016/s1290-0729(01)01297-2.
Kaushik, S.C., Tyagi, S.K., Mohan, S., 2003. Performance evaluation of an irreversible Stirling heat engine cycle. Int. J. Ambient Energy 24 (3), 149–156. https://doi.org/10.1080/01430750.2003.9674917.
Kongtragool, B., Wongwises, S., 2006. Thermodynamic analysis of a Stirling engine including dead volumes of hot space, cold space and regenerator. Renew. Energy 31 (3), 345–359. https://doi.org/10.1016/j.renene.2005.03.012.
Li, X., Liu, B., Yu, G., Dai, W., Hu, J., Luo, E., Li, H., 2017. Experimental validation and numeric optimization of a resonance tube-coupled duplex Stirling cooler. Appl. Energy 207, 604–612. https://doi.org/10.1016/j.apenergy.2017.05.123.
Li, Z., Haramura, Y., Tang, D., Guo, C., 2015. Analysis on the heat transfer characteristics of a micro-channel type porous-sheets Stirling regenerator. Int. J. Therm. Sci. 94, 37–49. https://doi.org/10.1016/j.ijthermalsci.2015.02.011.
Liao, T., Lin, J., 2015. Optimum performance characteristics of a solar-driven Stirling heat engine system. Energy Convers. Manag. 97, 20–25. https://doi.org/10.1016/j.enconman.2015.03.027.
Newman, W., Buckmaster, D., 2011. In: Stirling Duplex System Modeling for Control System Analysis, 9th Annual International Energy Conversion Engineering Conference (San Diego, California).
Penswick, L.B., Urieli, I., 1984. In: Duplex Stirling Machines, 19th Annual Intersociety Energy Conversion Engineering Conference, pp. 1823–1828. San Francisco, California.
Razani, A., Dodson, C., Roberts, T., 2010. A model for exergy analysis and thermodynamic bounds of Stirling refrigerators. Cryogenics 50 (4), 231–238. https://doi.org/10.1016/j.cryogenics.2009.12.007.
Tlili, I., Timoumi, Y., Nasrallah, S.B., 2008. Thermodynamic analysis of the Stirling heat engine with regenerative losses and internal irreversibilities. Int. J. Engine Res. 9 (1), 45–56. https://doi.org/10.1243/14680874jer01707.
Wu, F., Chen, L., Wu, C., Sun, F., 1998. Optimum performance of irreversible stirling engine with imperfect regeneration. Energy Convers. Manag. 39 (8), 727–732. https://doi.org/10.1016/s0196-8904(97)10036-x.